# Effect of Fiber Reinforcement on the Strength of Geopolymerised Soil: An Experimental Investigation and Numerical Modeling

**Mazhar Syed** [iD]**, Yash V. Kasat, Gaurav B. Sarda, and Anasua GuhaRay** [iD]

## 1   Introduction

The dual nature of black cotton soil (BCS) exhibits low volumetric stability upon moisture imbalance, leading to cause destruction of lightweight structures founded on them. Convention cementitious binders like lime and cement are the most utilizable binders for strengthening the geoengineering characteristics of expansive soils and efficiently reduce the problems associated with swelling and shrinkage. The production of these binders, however, contributes 7–8% of annual greenhouse gases around the world. The global demand for portland cement-based (PC) binders has increased and can reach up to 200% by the end of 2050 [1]. Usage of low carbon emission binders such as Alkali Activated Binder (AAB) is an alternative cementitious product for effectively reinforcing the soil. Typically, AAB is a long-chain polymeric sodium aluminosilicate compound, synthesized from alumina and silica-rich precursors through geopolymerisation [2]. AAB helps to eliminate the demand for Portland cement binders by overcoming the issue of disposing of fly ash and slag, thereby saving the related costs during landfills. In terms of energy, costs, and environmental impacts, AAB is recorded to produce almost 80% less $CO_2$ compared to Portland cement. In comparison, AAB's global warming potential is 70% lesser than the PC-based binders [3]. AAB also possessed early strength gain with low hydration heat, the higher resistance to acid and sulfate attack, excellent durability, improved freeze-thaw resistance, superior workability, and binding properties relative to hardened cement binders [4]. A substantial amount of progress was recorded over the last decades in applying geopolymerisation in ground improvement [5–7]. Although the aluminosilicate precursor-based AAB-treated soils efficiently enhance the compressive shear strength, but it exhibits weak tensile and flexure resistance. The existence

M. Syed · Y. V. Kasat · G. B. Sarda · A. GuhaRay (✉)
BITS-Pilani Hyderabad Campus, Secunderabad 500078, Telangana, India
e-mail: guharay@hyderabad.bits-pilani.ac.in

of shrinkage cracking is crucial in the summer season when this type of soil is encountered. The problem of shrinkage cracking can be effectively dealt with by including discrete fibers [8, 9]. Over the last few years, discrete fibers (natural/artificial) gained popularity in cemented soil stabilization owing to their higher tensile and durability [10, 11]. However, not many studies were conducted to compare the geomechanical behavior of both natural/artificial fiber-reinforced AAB soils. In the present study, an effort has been made to compare the geoengineering characteristics between polypropylene fiber (PF) and chemically modified coir fiber (TCF) reinforced AAB treated soil at different fly ash-slag proportions. To determine the effectiveness of both fiber-AAB-soil mixtures, a series of microstructural and geotechnical tests are conducted at different dosages of fibers. Based on the experimental results, a numerical analysis is performed using commercially available finite element software to correlate the flexural failure patterns for both PF and TCF reinforced soil beam.

## 2    Materials and Methods

### 2.1    Raw Materials

Black cotton soil (BCS) was collected from the Nalgonda region of Telangana state, while class F fly ash and slag were directly obtained from Ramagundam National Thermal Power plant and JSW Cement Ltd., Andhra Pradesh, respectively. BCS was classified as high plasticity clay (CH) according to the Unified Soil Classification System (USCS) and found to contain 78% clay. A constant length of 12 mm length of polypropylene and 25 mm length for coir fiber were obtained from Go-green product industries, Tamil Nadu. Coir fiber was chemically treated with 10 M of NaOH before inclusion as soil reinforcement. The different physicochemical and engineering properties of raw materials are provided in Table 1 as per ASTM codes.

**Table 1**  Properties of raw materials

| Soil Properties | Values | Fiber | PF | CF |
|---|---|---|---|---|
| Specific gravity | 2.65 | Diameter ($\mu$m) | 33 | 30 |
| Free swell index (%) | 88.30 | Density (g/cc) | 0.91 | 0.88 |
| Moisture content (%) | 24.0 | Cellulose (%) | – | 45 |
| Liquid limit (%) | 62.0 | Hemicellulose (%) | – | 1 |
| Plasticity index (%) | 38.0 | Lignin (%) | – | 48 |
| Dry density (g/cc) | 1.65 | Ash (%) | – | 3 |
| Tensile strength (kPa) | 25.8 | Tensile strength (mPa) | 330 | 94 |
| Compression strength (kPa) | 187 | Elastic modulus (mPa) | 350 | 330 |
| Flexural strength (kPa) | 100 | Melting Point ($^0$C) | 168 | – |

## 2.2 Alkali Activated Binder (AAB)

AAB was prepared by mixing sodium silicate, sodium hydroxide, and aluminosilicate precursors (fly ash and slag) with a mass ratio of 129:10.57: 400 [3, 12]. Both sodium silicate and sodium hydroxide chemicals were obtained from Hychem Chemicals Ltd. in the form of solution and pellets, respectively. Fly ash and slag proportions were varied in the AAB mixture to obtain an optimum mix.

## 2.3 Sample Preparation

BCS was uniformly mixed with 5% of AAB paste (total dry mass of soil) by varying fly ash and slag content with a constant 0.4 w/s ratio in the chemical binders. AAB blended soil was compacted in a container of $(950 \times 480 \times 150)$ mm in 3 layers with a 9 kg steel rammer under a free fall of 310 mm. The compacted soil was covered with moist jute bags for up to 48 h to remove excess heat during the geopolymerization reaction. Prior to mixing either PF or TCF (0.5 and 1% by mass of soil) in the AAB-treated BCS, it was oven-dried. A series of microstructural and geotechnical tests were performed for both fiber-AAB composite BCS.

## 2.4 Geotechnical Characteristics

A series of microstructure and geotechnical tests were performed on both untreated soil and fiber-reinforced AAB mixed soil. The influence upon the addition of PF and TCF in AAB treated soil was analyzed through unconfined compressive strength split tensile strength (STS) and flexure strength tests. UCS test on both untreated soil and fiber-reinforced AAB treated soils were conducted as per ASTM D2166 [13] standard by compacting them in a split cylindrical mold of 76 mm height with an inner diameter of 38 mm at their MDD-OMC values, respectively. A static strain rate of 1.25 mm/min was maintained throughout the test.

STS tests were conducted as per ASTM D3967 [14] on the Marshal Stability machine by attaching a loading strip of 12.5 mm on the load frame with a constant strain rate of 50.5 mm/min. Both AAB treated and fiber-reinforced soils were compacted in a cylindrical mold of 100 mm diameter and 80 mm thickness. The following formula calculates split tensile strength $(S_t)$

$$S_t = 2p/td\, \Pi \tag{1}$$

where
   P = ultimate load at which failure of sample occurred (N),
   t = thickness of specimen (mm),
   d = diameter of the specimen (mm).

The flexure strength test was conducted using a three-point bending flexure machine as per ASTM D-1635 [15] standard by molding a soil beam of 280 mm × 70 mm × 70 mm into five layers with a 3 kg steel rammer under a free fall of 310 mm. Flexural strength tests ($S_f$) mPa calculated by using the formula as follow.

$$S_f = 3pl/2bh^2 \qquad (2)$$

P = ultimate breaking load at which sample failure occurred (N),
l = length of support on beam specimen (mm),
b = width of the beam specimen (mm), h = depth of the beam specimen (mm).

## 2.5 Numerical Modeling

The soil beam was simulated using three-point bending flexure in commercially available finite element software ABAQUS. The basic soil, AAB, and fiber material properties (such as elastic modulus, Poisson ratio, and c-φ parameters) were used in the finite element model to track flexural resistance variations. In addition, the soil beam was assumed to be an elastic material, and rigid supports were provided. To demonstrate the flexural behavior of the soil beam, a load versus deflection chart was developed and compared with the experimental results.

# 3 Results and Discussion

## 3.1 Fourier Transform Infrared Spectroscopy (FTIR)

FTIR molecular bonding was analyzed using a JASCO FTIR 4200 setup with K.Br. Pellet arrangement under 4000-400 $cm^{-1}$ spectral range. O-H stretching vibrations' transmittance peaks were found around 3600 $cm^{-1}$ for both untreated and AAB-treated soils in Fig. 1. A slight reduction in the intensity of AAB and fiber-reinforced soils was found at 3600 $cm^{-1}$, followed by the O-H hydroxyl alcohol group at 3420 $cm^{-1}$. This marginal change in bonding may be due to clay particles' chemical weathering action [16, 17]. The broadband detected at 1630 $cm^{-1}$, and 1440 $cm^{-1}$ correspond to $C = C$ alkene and $CH_2$ bending vibrations in both fiber-reinforced soil. This carbonation reaction may be induced due to cellulose's active existence in the fiber alkaline matrix [12]. Moreover, a sharp band attributed to Si-O-Si's asymmetric stretching vibration around 1050 $cm^{-1}$ in the clay particles. The combined mixture of aluminosilicate compounds and fiber alkalinity in the soil showed a broader peak of (Al)-O bending vibration at 790 $cm^{-1}$ along with the Si-O stretching group around 510-490 $cm^{-1}$, respectively. Thus, the spectrum peaks from untreated soil, AAB,
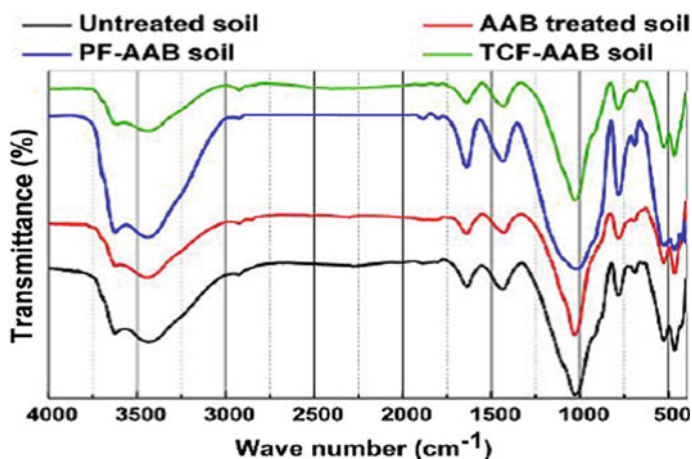
**Fig. 1** FTIR spectroscopy of untreated and fiber AAB-treated soil

and fiber-reinforced AAB treated soil showed similar bonds with a chemical shift of about 10 cm$^{-1}$.

## 3.2 Stereomicroscope and SEM Images

The soil's physical features were captured at different magnifications using the stereomicroscope of SX27 Olympus with the least dimension of 20 µm. Surface micrographs were captured using a Thermo Scientific Apreo SEM provided by Field Electron-Ion Company. 20 kV excitation voltage with the help of the Gentle beam of electromagnetic lenses was adapted to screen the surface. Figure 2a–h displayed the stereomicropic and SEM images of untreated, AAB treated, and fiber-reinforced AAB soil, respectively. Untreated soil revealed a light brownish color region, which indicated the occurrence of the smectite group. Irregular aggregated particles in the form of vitreous texture were observed with minor surface cracks in Fig. 2a–b. The hardened AAB paste deposit by filling the pores between the clay particles was observed in Fig. 2c. Moreover, a series of spherical particles with different sizes were detected in Fig. 2d. The occurrences of irregular hallow spherical particles on the soil surfaces might be due to the presence of fly ash. Figure 2e–f showed the densely compacted microstructure of the PF-AAB soil matrix, which interlocked the particles by forming a spatial thread groove network [8]. The vigorous morphology changes were also noticed in TCF-AAB soil in Fig. 2g–h which acts as bridge surfaces. Thus, the combined fiber-AAB-soil mixtures aid in controlling the tensile cracking behavior with a higher linkage effect.
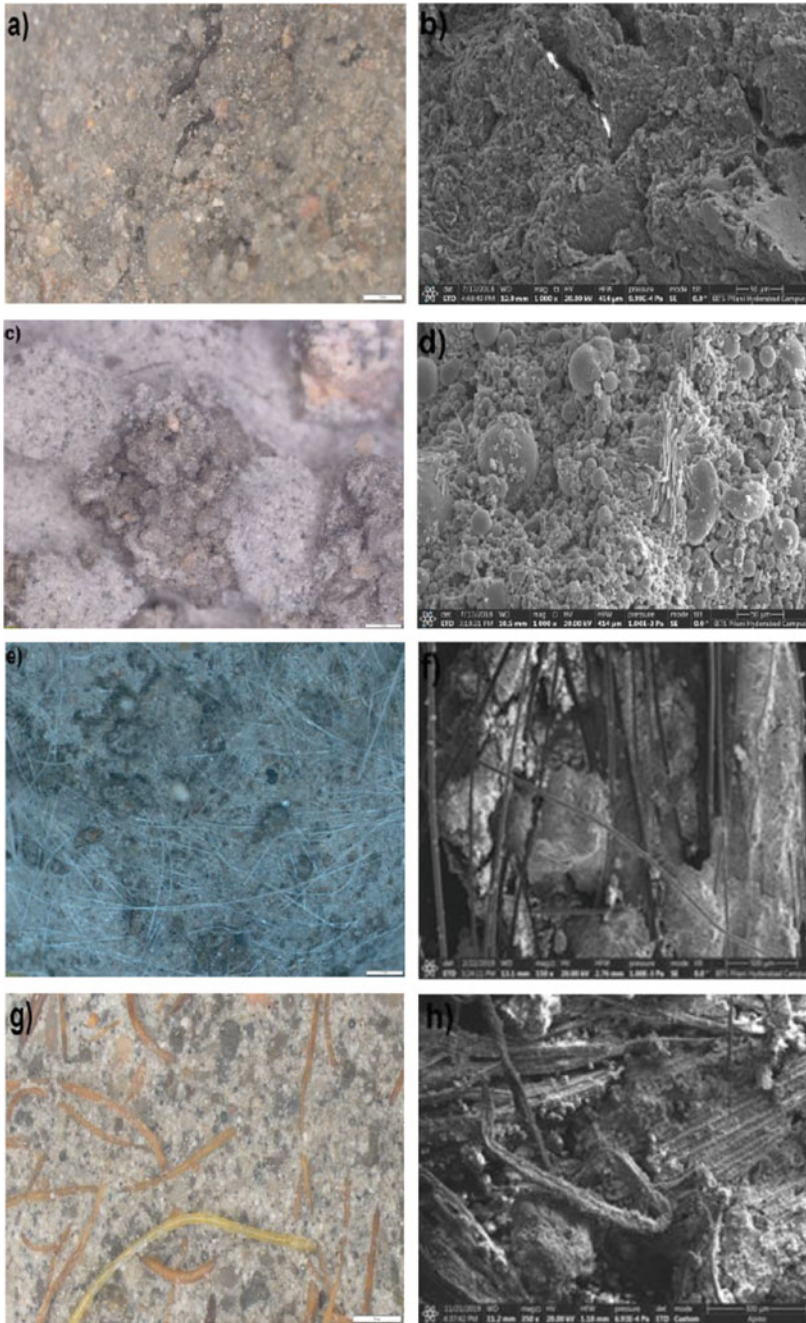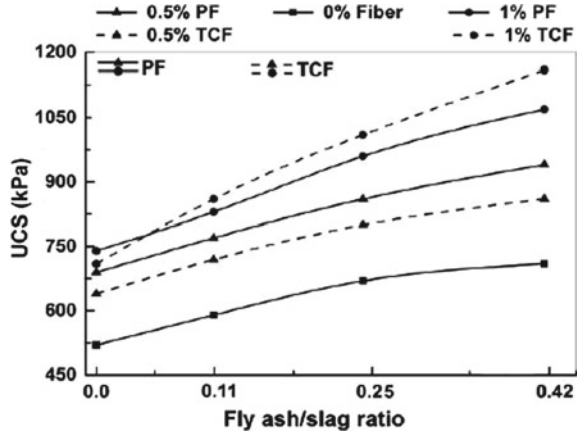
**Fig. 2** Stereomicroscopic and SEM images of **a–b** Untreated soil, **c–d** AAB treated soil, **e–f** PF-AAB treated soil, **g–h** TCF reinforced AAB soil

**Fig. 3** Variation of UCS for
PF and TCF reinforced AAB
treated soil at different fiber
dosages



## 3.3 Unconfined Compression Strength (UCS)

Figure 3 plotted UCS of two kinds of fiber-reinforced AAB soil at varying fibers and
fly ash-slag ratio. The solid lines indicated the PF-AAB, and dotted lines represented
the TCF-AAB-soil mixture. The figure revealed that the combined addition of fibers
in the fly ash slag-based AAB soils had a significant effect on the rate of compressive
shear strength gain. As the replacement of fly ash with slag content increased, the
rate of geopolymerisation reaction and confinement bonding efficiency of soil-fiber
was greatly enhanced. Moreover, PF-AAB UCS increased by over 15% compared
to TCF-AAB at lower fiber dosages. The relative gain in PF's shear strength upon
TCF reinforced AAB soil might be attributed to the development of higher interfacial
surface roughness, which mobilized the friction during loading [9, 11]. It was also
interesting to note that TCF's initial addition did not cause much impact on stiffness
behavior. The combined effects of TCF (beyond 0.5%) and 70/30 fly ash/slag attained
higher shear strength among all compositions. In addition, the marginal improvement
was observed in the PF-AAB reinforced soil at a higher dosage (1%) in the soil. This
might be due to smooth surface texture formation, which does not easily allow the
soil to compact [8, 18]. Thus, the combined addition of fibers in AAB can efficiently
enhance the compression shear strength with higher linkage effects.

## 3.4 Split Tensile Strength (STS)

Figure 4 showed the tensile strength of fiber-reinforced soil specimens with varying
fly ash-slag and fiber dosages. It was found that, when the fiber dosage was constant,
the ITS results for AAB soils were almost similar, regardless of the fiber type and
fly ash/slag proportions. The gain in tensile strength followed a parallel pattern to
that of UCS for both PF and TCF reinforced soils. Upon comparison, the PF-AAB

**Fig. 4** Variation of STS for
PF and TCF reinforced AAB
treated soil at different fiber
dosages
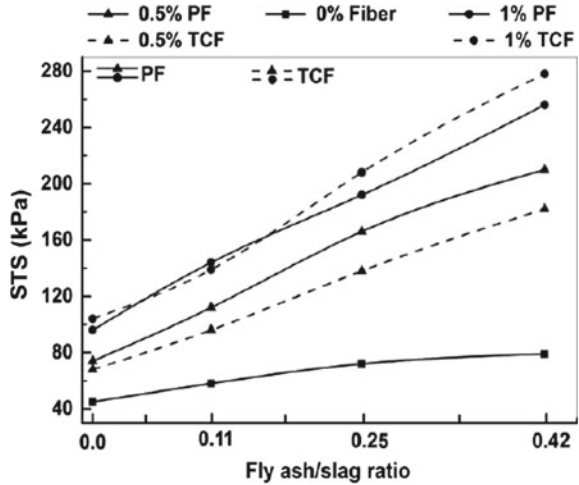


showed greater stretching and interlocking density over TCF-AAB soil mixtures. This beneficial effect of PF reinforcement might be attributed to its higher interfacial frictional resistance across the soil cementing matrix [10, 18]. Furthermore, PF had actively regulated the strain cracks along soil fiber's failure plane by producing a spatial thread groove network. Hence, the increase in slag dosages with fiber reinforcement in the AAB soil aided by strengthening the tensile resistance capacity and restricting the relative movement of fiber.

## 3.5 Flexural Strength ($S_f$)

Figure 5a plotted flexural strength of PF and TCF reinforced at two different percentages (0.5 and 1%) in the fly ash-slag-based AAB soils. It can be seen that both fibers enhanced the rate of increase in flexural resistance with an increase in slag and fiber dosages. The improvement was much more significant in PF-AAB soil relative to the TCF-AAB-soil mixture. The relative gain in flexural and shear strength in PF reinforced soil might be due to their higher contact area (confinement bonding) and frictional resistance [19, 20]. Moreover, slag-based AAB had the potential to reinforce the soils through active cementation compounds due to the rapid dissolution of pozzolanic precursors in the presence of reactive alumina and silica soil substances. Thus, the vigorous changes in soil fiber interlocking density and surface morphology enhanced the flexural resistance potentially. Figure 5b shows the schematic soil beam arrangement and load supports.
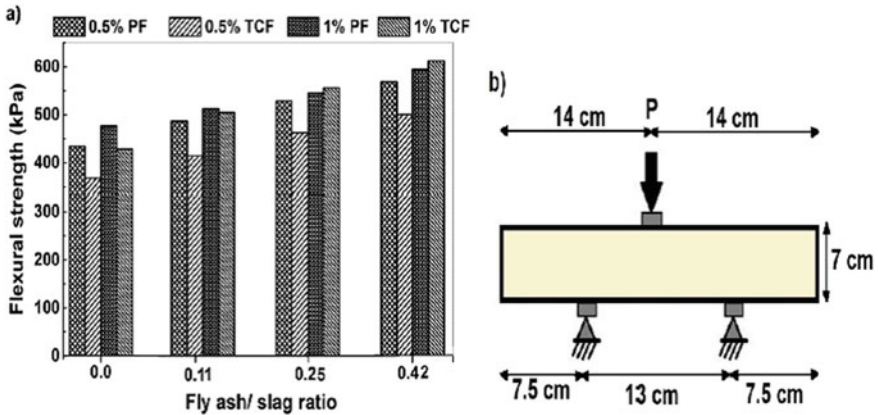
**Fig. 5** **a** Variation of flexural strength for PF-TCF-AAB soil **b** Typical flexural soil beam set up

### 3.5.1 Finite Element Model

Figure 6 shows the three-point bending soil flexural beam model before the application of load. The meshed 2.5 mm × 2.5 mm soil beam was shown in Fig. 6a. As the load's application increased, the soil beam significantly deformed and failed at the midpoint on the beam's bottom side. A maximum 4.5 mm deflection for untreated soil occurred at the midpoint, which was shown in Fig. 6b. Similar studies are carried out for TCF-AAB and PF-AAB soil. Figure 7 showed the load-deflection curve obtained from the experimental and finite element analysis of untreated soil, TCF, and PF reinforced AAB soil beam. The results of the finite element analysis indicated a good correlation with that of the experimental results.
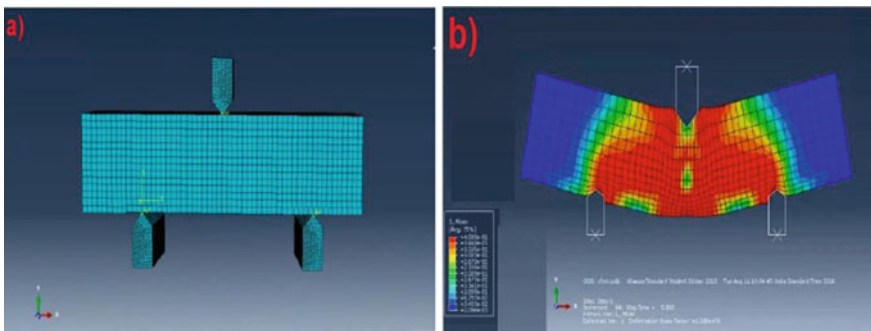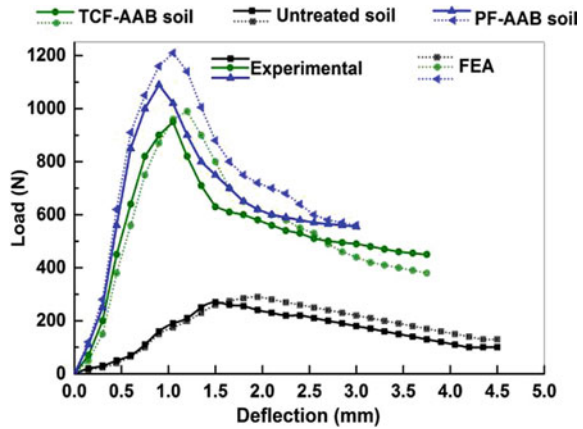


**Fig. 6** **a** Load actuator soil beam model setup **b** Soil beam deflection at mid-span

**Fig. 7** Variation of flexural
load and deflection curve for
soil beam



## 4 Conclusions

The present experimental study investigated the effects of fiber reinforcement in
alkali-activated binder (AAB) treated expansive soil. The following conclusions can
be drawn from this analysis:

1. The PF-AAB soil showed higher strength performance than the TCF-AAB-soil
   mixture. UCS and STS of AAB-BCS increased by 48% and 38% for PF, and
   39% and 33% for TCF reinforced soil when the fiber dosages were low.
2. Greater mobilization of friction and interfacial bonding helped PF to yield higher
   mechanical strength performance than TCF-AAB-soil, irrespective of dosage
   of fiber and slag in the AAB compound.
3. The combined addition of AAB and fiber had a significant effect on the rate of
   gain of flexural strength; these values notably increased with fiber dosages and
   fly ash/slag ratio.
4. Micrographs of fiber-AAB soils revealed new surface morphology, and it can
   act as a spatial thread-bridge network, which improves the particle holding and
   interlocking density around the fiber surfaces.
5. PF-AAB soil mixture attained the highest flexural strength upon TCF-AAB soil
   mixture. At higher fiber dosages, both PF and TCF play a substantial role in
   regulating flexure crack development.
6. The flexural failure pattern obtained from the finite-element model showed
   similar trends to that of the physical test failure in the laboratory.

# References

1. Taylor, M., Tam, C., Gielen, D.: Energy efficiency and CO2 emissions from the global cement industry energy efficiency and CO2 emission reduction potentials and policies in the cement. IEA-WBCSD Workshop, pp. 4–5 (2006)
2. Davidovits, J.: Properties of geopolymer cements, Alkaline Cements and Concretes, Kiev, Ukraine, pp. 1–19 (1994). https://doi.org/10.1073/pnas.0811322106
3. Mazhar, S., Guharay, A.: Stabilization of expansive clay by fibre-reinforced alkali-activated binder: an experimental investigation and prediction modelling (2020). https://doi.org/10.1080/19386362.2020.1775358
4. Provis, J.L., van Deventer, J.S.J.: Alkali Activated Materials, 13th ed. Springer International Publishing, UK (2014). https://doi.org/10.1007/978-94-007-7672-2
5. Miao, S., Wei, C., Huang, X., Shen, Z., Wang, X., Luo, F.: Stabilization of highly expansive black cotton soils by means of geopolymerization. J. Mater. Civ. Eng. **29**, 04017170 (2017). https://doi.org/10.1061/(asce)mt.1943-5533.0002023
6. Komljenović, M., Baščarević, Z., Bradić, V.: Mechanical and microstructural properties of alkali-activated fly ash geopolymers. J. Hazard. Mater. **181**, 35–42 (2010). https://doi.org/10.1016/j.jhazmat.2010.04.064
7. Murmu, A.L., Dhole, N., Patel, A.: Stabilisation of black cotton soil for subgrade application using fly ash geopolymer. Road Mater. Pavement Design. **0**, 1–19 (2018). https://doi.org/10.1080/14680629.2018.1530131
8. Tang, C., Shi, B., Gao, W., Chen, F., Cai, Y.: Strength and mechanical behavior of short polypropylene fiber reinforced and cement stabilized clayey soil. Geotext. Geomembr. **25**, 194–202 (2007). https://doi.org/10.1016/j.geotexmem.2006.11.002
9. Consoli, N.C., Arcari Bassani, M.A., Festugato, L.: Effect of fiber-reinforcement on the strength of cemented soils. Geotext. Geomembr. (2010). https://doi.org/10.1016/j.geotexmem.2010.01.005
10. Sudhakaran, S.P., Sharma, A.K., Kolathayar, S.: Soil stabilization using bottom ash and areca fiber: experimental investigations and reliability analysis. J. Mater. Civ. Eng. **30**, 1–10 (2018). https://doi.org/10.1061/(ASCE)MT.1943-5533.0002326
11. Moghal, A.A.B., Chittoori, B.C.S., Basha, B.M., Al-Shamrani, M.A.: Target reliability approach to study the effect of fiber reinforcement on UCS Behavior of lime treated semiarid soil. J. Mater. Civ. Eng. **29**, 04017014 (2017). https://doi.org/10.1061/(asce)mt.1943-5533.0001835
12. Gupta, S., GuhaRay, A., Kar, A., Komaravolu, V.P.: Performance of alkali-activated binder-treated jute geotextile as reinforcement for subgrade stabilization. Int. J. Geotech. Eng. 1–15 (2018). https://doi.org/10.1080/19386362.2018.1464272
13. ASTM D 2166: Standard test method for unconfined compressive strength of cohesive soil (2006)
14. ASTM D 3967: Standard Test Method for Splitting Tensile Strength of Soil Specimens, ASTM D3967 West Conshohocken, PA (2016)
15. ASTM D1635: Standard Test Method for Flexural Strength of Soil-Cement Using Simple Beam with Third-Point Loading, ASTM D1635West Conshohocken, PA (2019)
16. Adhikari, B., Khattak, M.J., Adhikari, S.: Mechanical and durability characteristics of flyash-based soil-geopolymer mixtures for pavement base and subbase layers. Int. J. Pavement Eng. **0**, 1–20 (2019). https://doi.org/10.1080/10298436.2019.1668562
17. Mwaikambo, L.Y., Ansell, M.P.: Chemical modification of hemp, sisal, jute, and kapok fibers by alkalization. J. Appl. Polym. Sci. **84**, 2222–2234 (2002). https://doi.org/10.1002/app.10460

18. Pourakbar, A.: Application of alkali-activated agro-waste reinforced with wollastonite fibers in soil stabilization. J. Mater. Civ. Eng. **29**, 04016206 (2016). https://doi.org/10.1061/(asce)mt. 1943-5533.0001735
19. Anggraini, V., Asadi, A., Farzadnia, N., Jahangirian, H., Huat, B.B.K.: Reinforcement benefits of nanomodified coir fiber in lime-treated marine clay. J. Mater. Civ. Eng. **28**, 1–8 (2016). https://doi.org/10.1061/(ASCE)MT.1943-5533.0001516
20. Correia, A.A.S., Venda Oliveira, P.J., Custódio, D.G.: Effect of polypropylene fibres on the compressive and tensile strength of a soft soil, artificially stabilised with binders. Geotext. Geomembr. **43**, 97–106 (2015). https://doi.org/10.1016/j.geotexmem.2014.11.008